1 **A dedicated robust instrument for water vapor generation at low humidity for use with a laser water**

2 **isotope analyzer in cold and dry polar regions.**

4 Christophe Leroy-Dos Santos[1], Mathieu Casado[1,2], Frédéric Prié[1], Olivier Jossoud[1], Erik Kerstel[3], Samir

5 Kassi[3], Elise Fourré[1], Amaëlle Landais[1, *]

7 [1] Laboratoire des Sciences du Climat et de l'Environnement, CEA-CNRS-UVSQ-Paris Saclay-IPSL, Gif-sur-

8 Yvette, France

9 [2] Alfred Wegener Institut, Helmholtz Center for Polar and Marine Research, Potsdam, Germany

10 [3] Laboratoire Interdisciplinaire de Physique, CNRS - Université Grenoble Alpes, Grenoble, France

11 [*] corresponding author: amaelle.landais@lsce.ipsl.fr

13 **Abstract**

14 Obtaining precise continuous measurements of water vapor isotopic composition in dry places (polar or

15 high-altitude regions) is an important challenge. The current limitation is the strong influence of humidity

16 on the measured water isotopic composition by laser spectroscopy instruments for low humidity levels

17 (below 3000 ppmv). This problem is addressed by determining the relationships between humidity and

18 measured $\delta^{18}O$ and δD of known water standards. We present here the development of a robust field

19 instrument able to generate water vapor, down to 70 ppmv, at very stable humidity levels (average 1σ

20 lower than 10 ppmv). This instrument, operated by a Raspberry interface, can be coupled to a commercial

21 laser spectroscopy instrument: it turned to be very stable in an autonomous mode during more than one

22 year at the East Antarctic Concordia station.

23

24

25 **1. Introduction**

26 The recent development of laser spectroscopy instruments now enables the continuous measurement of

27 the isotopic composition of water vapor at many observation stations all around the world (Bailey et al.,

28 2015; Bastrikov et al., 2014; Schmidt et al., 2010; Sodemann et al., 2017; Tremoy et al., 2011). In particular,

29 the isotopic composition of the water vapor has proven to be a very useful tool to document moist synoptic

30 events in many locations (Bonne et al., 2014; Guilpart et al., 2017). In polar regions, the water vapor

31 isotopic signal is not only useful to detect the origin of moist air (Bréant et al., 2019; Kopec et al., 2014)

32 but also to improve the interpretation of the isotopic composition of water in surface snow and ice core

33 archives (Steen-Larsen et al., 2014). Indeed, exchanges are occurring after deposition between the surface

34 snow and the water vapor leading to modifications of the isotopic composition of the former and hence

35 of the archived ice (Casado et al., 2016, 2018; Ritter et al., 2016).

36   Obtaining continuous measurements of the water vapor isotopic composition at Concordia station in

37   central Antarctica is a key scientific challenge since the deep ice core drilled there, EPICA Dome C, provides

38   the oldest continuous water isotopic record to date (Jouzel et al., 2007). It is thus a key reference for the

39   study of past climate, and a correct interpretation of the isotopic record relies on the quantification of the

40   transfer function between climate parameters and water isotopic composition in ice, itself influenced by

41   exchanges with water vapor in the upper layers of the firn (Casado et al., 2018). Such knowledge is also of

42   uttermost importance for the interpretation of water isotope records from the starting deep drilling

43   project "Beyond EPICA-Oldest Ice" (https://www.beyondepica.eu), whose aim is to drill a 1.5-million-year

44   old ice core on the Little Dome C site located 40 km away from Concordia station, hence with similar low

45   temperature and humidity conditions.

46   One of the main limitations of the current commercial instruments when deployed in polar regions is their

47   relatively poor performance at low water vapor concentration. Generally, the precision of the measured

48   isotopic ratios $\delta^{18}O$ and δD rapidly worsens when the water mixing ratio decreases to humidity levels

49   below 3,000-5,000 ppmv (part-per-million per volume) (Bonne et al., 2014; Weng et al., 2020). However,

50   in remote continental areas in Greenland and Antarctica, temperatures in winter can drop to very low

51   values, leading to humidity levels down to 10 ppmv (Genthon et al., 2017). Arguably one of the most

52   extreme experiments for continuous measurement of the water vapor isotopic composition was probably

53   the deployment of a commercial Picarro L2130-i instrument at the East Antarctic French-Italian station of

54   Concordia where the mean annual temperature is around -54°C and the humidity barely exceeds 1000

55   ppmv during the warmest summer days (Casado et al., 2016). For such applications, there are two major

56   impacts of low humidity on the raw isotopic signal: first, we generally observe an apparent increase in the

57   $\delta^{18}O$ and δD with decreasing humidity level and second, the standard deviation associated with the

58   continuous measurements of $\delta^{18}O$ and δD of the water vapor increases. It can thus lead to overall

59   uncertainties of several ‰ for $\delta^{18}O$ and tens of ‰ for δD. It is thus of uttermost importance to have a

60   correct determination of the humidity dependency of the water vapor isotopic ratios.

61   Commercial instruments from Picarro Inc. are usually associated with a Picarro Standard Delivery Module

62   (SDM) dedicated to generate humidity at stable levels between 5,000 and 30,000 ppmv. Using such a set-

63   up for humidity levels below 5,000 ppmv leads to large uncertainties in the determination of the humidity

64   influence on the water vapor isotopic composition (e.g. Guilpart et al., 2017). These uncertainties are due

65   both to the instability of the water vapor generation using the SDM (in terms of water concentration –

66   humidity— and/or isotopic composition) and due to the analytical noise in the spectroscopy

67   measurements when the absorption signals are weak. An alternative commercial device is the LGR (Los

68   Gatos Research) calibration system (water vapor isotope standard source, WVISS), which uses a nebulizer

69   to instantaneously evaporate micro-droplets of liquid water from a standards reservoir into a large (1 L)

70   vaporizing chamber (Dong and Baer, 2010) This system is very stable and well adapted for humidity range

71   between 2,500 and 25,000 ppmv (Aemisegger et al., 2012).

72   Several home-made water vapor injection systems have been developed with the specific aim to achieve

73   a better stability of the generated humidity at low humidity levels. A first approach is to use a dew point

74   generator injecting small amounts of water into dry air (Lee et al., 2005; Wang et al., 2009). This approach

75   is time consuming to reach equilibrium and relies on a very precise knowledge of the temperature to

76   calculate the isotopic fractionation. A method using a piezoelectric microdroplet generator into a dry air

77   stream could generate water mixing ratios at humidity levels between 12 and 3,500 ppmv (Iannone et al.,

78   2009; Sturm and Knohl, 2009). However, adjustment of humidity level and long-term stability were difficult

79   to obtain with such devices. Systems relying on the use of syringe pumps were also built by Gkinis et al.

80   (2010) and Tremoy et al. (2011): a small fraction of the input stream of liquid water is introduced into a

81   hot oven where water is vaporized in the presence of a dry air flow. These systems cover humidity range

82   between 2,000 and 30,000 ppmv. Finally, bubbler systems, in which dry air flows through a large volume

83   of water to create saturated vapor, are very robust but can only produce water vapor at high humidity

84   level (Ellehoj et al., 2013). The aforementioned devices are unfortunately not well suited for automatic

85   long-term operation at low humidity levels. During the 2014-2015 summer field season at Concordia

86   station in Antarctica, a home-made humidity generator specifically designed for low humidity levels

87   (Landsberg, 2014) has been deployed (Casado et al., 2016). The device used dual high-precision, low-

88   volume, syringe pumps to generate stable humidity levels at two different isotopic compositions over the

89   range from 100 to 800 ppmv (Casado et al., 2016). Unfortunately, we observed quite a large scattering

90   among the isotopic values measured at similar humidity levels, as well as a large discrepancy between the

91   humidity dependency of the water isotopic ratios measured in the field and that measured in the

92   laboratory. Upon return to the laboratory, these defaults were traced primarily to tiny leaks in the water

93   supply lines to the syringes.

94   Therefore, we re-engineered the prototype by Landsberg (2014) in order to develop a robust and

95   autonomous device for stable low level humidity generation for the purpose of precise humidity

96   calibration of spectroscopic instruments. This device has now been operating with minimum manual

97   intervention for more than one year at two polar stations in Antarctica, Dumont d'Urville and Concordia,

98   coupled to Picarro laser spectroscopy instruments. We detail here the technical description of the

99   instrument and show key performance characteristics, enabling, for instance, a discussion of small

100 amplitude signals such as the diurnal variability of the water vapor isotopic composition in remote dry

101 sites in East Antarctica.

102

103   **2.   New vapor generator for low humidity levels**

104

105 The low-humidity level generator (LHLG) developed here relies on the same principle as the one developed

106 by Landsberg (2014), i.e., a steady, undersaturated evaporation of a liquid water droplet at the tip of a

107 needle into a dry air stream inside a small evaporation chamber. Based on this first prototype, the

108 instrument has been remodeled including a specific hardware and software design.

109

110 **2-1-Physical principle**

111 The LHLG is based on undersaturated evaporation of a small droplet at the tip of a needle (Figure 1). Liquid

112 water is pushed through a needle around which dry air is flowing. Dry air is obtained from a bottle of high

113 purity synthetic air with pressure regulation through two manometers connected in series. The mass flux

114 of water f_L is kept low compared to the air mass flow f_A so that the relative humidity h of the downstream

115 moist air flow remains low ($h < 0.1$). Therefore, the air stays largely undersaturated and its humidity is

116 controlled only by the flow of liquid water in the needle and that of the dry air upstream of it. The mixing

117 ratio (or humidity) of the air as classically provided by a Picarro instrument is given by:

118

119 $MR = \frac{d_{H2O} \times f_L \times R \times T_{st}}{f_A \times P_{st} \times M_{H2O}}$ (1)

120

121 where d_{H2O} = 1000 kg.m^{-3} is the density of water, R = 8.314 J mol^{-1} K^{-1} is the universal gas constant, T_{st} =

122 293.15 K and P_{st} = 1.0.10^5 Pa are standard conditions of temperature and pressure and M_{H2O} = 18.10^{-3}

123 kg.mol^{-1}. Note that the flow of water f_L needs to be expressed in m^3.min^{-1} and the air flow f_A is expressed

124 in m^3.min^{-1} at 20 °C and 1 atm (standard cubic meter per minute).
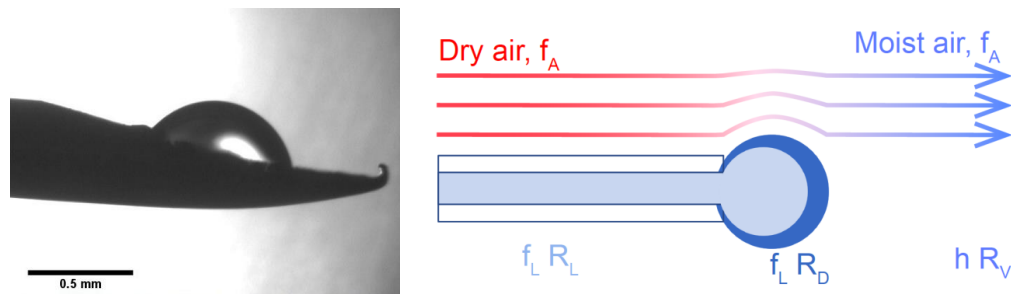
125

126 **_Figure 1_**: _Evaporation of a droplet in the humidity generator chamber: left, picture from the prototype from_

127 _Landsberg (2014); right, schematics of the water molecules being transferred to the air flow (Casado,_

128 _2016)._

129

130 Physically, when the flux of water or air is changed, there is first a transient regime during which the radius

131 of the droplet changes, modifying the evaporative surface and therefore the humidity of the outgoing air.

132   Once a stationary regime is reached, the radius of the droplet is stabilized and the humidity is given by

133   equation 1. In this regime, there is no accumulation of water molecules in the system and therefore the

134   isotopic composition of the vapor produced is equal to the isotopic composition of the liquid water

135   injected in the needle: $R_V = R_L$ (note that because of the fractionation during the transition phase, the

136   isotopic composition of the droplet R_D is necessarily different from R_L and R_V When changing the flux of

137   evaporating water, we modify the size of the evaporating surface and therefore the radius of the drop.

138   The evolution of the radius of the drop can be obtained from the resolution of a non-linear differential

139   equation of the volume V of the drop:

140

141    $$dV/dt = f_L - f_{evap} \tag{2}$$

142

143   where $f_{evap} = k_e \times S$ is the evaporation flux depending of k_e, the evaporation rate and S, the surface area of

144   the drop exposed to the dry air. A good approximation is to consider the shape of the drop as a fraction of

145   a sphere of variable radius intercepted by the surface of a disk of constant radius (the syringe tip). By

146   solving numerically the differential equation (2), it is possible to faithfully simulate the behavior of the

147   device under changing conditions. The isotopic composition is computed by the introduction of an

148   evaporation fractionation factor following Cappa et al. (2003). This numerical approach validates the

149   theoretical explanation of the undersaturated evaporation of the droplet. It is noted that in steady-state,

150   the isotopic composition of the generated water vapor does not depend on the injected flux of water, nor

151   on the specific humidity.

152

153   **2-2- Instrument conception**

154

155   -   **Technical realization**

156   As the LHLG relies on operating in a stationary regime, it is important that the dry air input and the water

157   input are steady. Thus, the air and water fluxes, as well as the air pressure in the evaporation chamber are

158   controlled by electronic PID regulators. The dry air flux is regulated by a high-precision mass flow controller

159   (Vögtlin GSC-A9TS-DD22) operating at a range from 6 to 600 sccm (std cm^3 min^{-1}) and an accuracy of 3.3

160   sccm. The water flux is regulated by a high-precision syringe pump (Harvard Apparatus Pump 11 Pico Plus

161   Elite Dual), which can produce a water flow down to 10.8 pL min^{-1} with an accuracy of 0.35 % using syringes

162   with a volume ranging from 10 µL to 250 µL. We operate in the routine mode with a dry air flow of 300

163   sccm and a water flow between 0.02 to 0.5 µL min^{-1} using mainly 50 or 100 µL syringes. A single pump is

164   equipped with two syringes that provide two water flows into two evaporation chambers in parallel

165   (Figures 2 and 3). Each syringe is connected to a water reservoir and to an evaporation chamber by a

166   double 3-way liquid valve (Rheodyne MXX777603) switching from an "infuse" mode to a "refill" mode.

167   A major change to the instrument designed by Landsberg (2014) is the introduction of this double 3-way

168   valve with leak tight connections and an internal volume of 1.9 μL. This modification is an important

169   improvement as it enables automatic handling of the standards from a reservoir to the evaporation

170   chamber with a robust connection, avoiding in particular potential air bubbles in the water flow. Indeed,

171   the compressibility of air bubbles trapped in the water flow can lead to flow irregularities by amplification

172   of small non-linearities in the progression of the syringe plunger. This will lead to non-steady state

173   operation, which in turn creates artefacts in the humidity and isotopic composition, reducing the

174   performance of the calibration device. In addition, the 3-way valve provides the opportunity of a "refill"

175   mode in which the syringes draw standard water from a reservoir. When equipped with 100-μL syringes,

176   the instrument can operate for several hours up to one day between refills. With the addition of the auto-

177   refill option and the effective suppression of bubbles, the instrument can be used unattended for many

178   months, as required for an Antarctic winter field campaign.

179
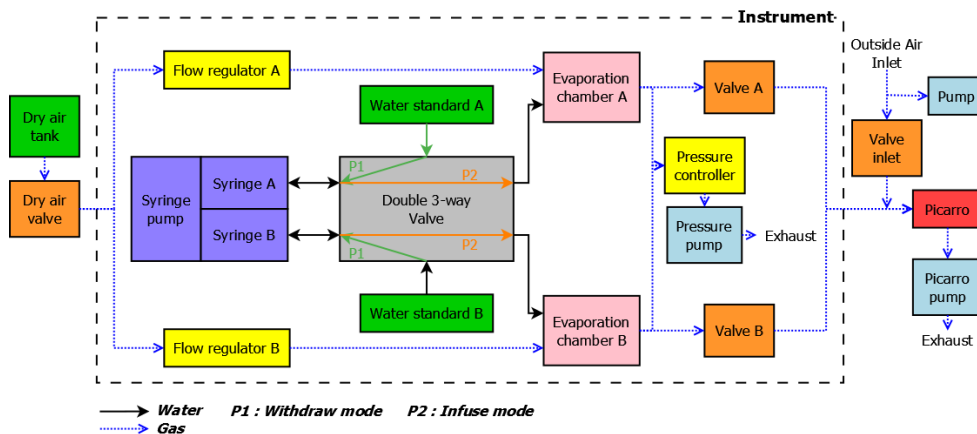
180

181   *Figure 2*: Humidity generator schematic diagram

182

183   The evaporation chambers are stainless steel cylinders equipped with specific connectors (Swagelok Ultra-

184   Torr SS-4CD-TW-25) holding silicon rubber septa through which needles are inserted toward the middle of

185   the chamber. The pressure in both chambers is regulated by a pressure controller (Bronkhorst P-702CV-

186   1K1A-AAD-22-V) with a precision of 3 mbar in a range from 0 to 1,000 mbar. This pressurization of the two

187   chambers combined with the relatively high flow (higher than required by the infrared spectrometers)

188   enables maintaining a steady state whether or not the infrared spectrometer is connected, and increases

189   the time efficiency of calibration procedures. The control of the instrument is ensured by a Rasberry Pi

190   that can be interfaced to the L2130-i in sequencer mode (see below).

191   The hardware has been designed to meet the specifications dictated by field conditions: 1) All components

192   are fixed in a transportable case (except the dry air bottle), isolated from vibration by an anti-vibration

193   foam. 2) A panel of connectors (HDMI, USB, Ethernet, etc.) ensures the accessibility to the instrument

194   when it is closed. 3) The electrical and electronic parts (e.g. power supply, Raspberry Pi) are separated

195   from the rest of the instrument (e.g. sensors, gauges). Both the electrical and electronic parts are fully and

196   easily accessible in case of failure.
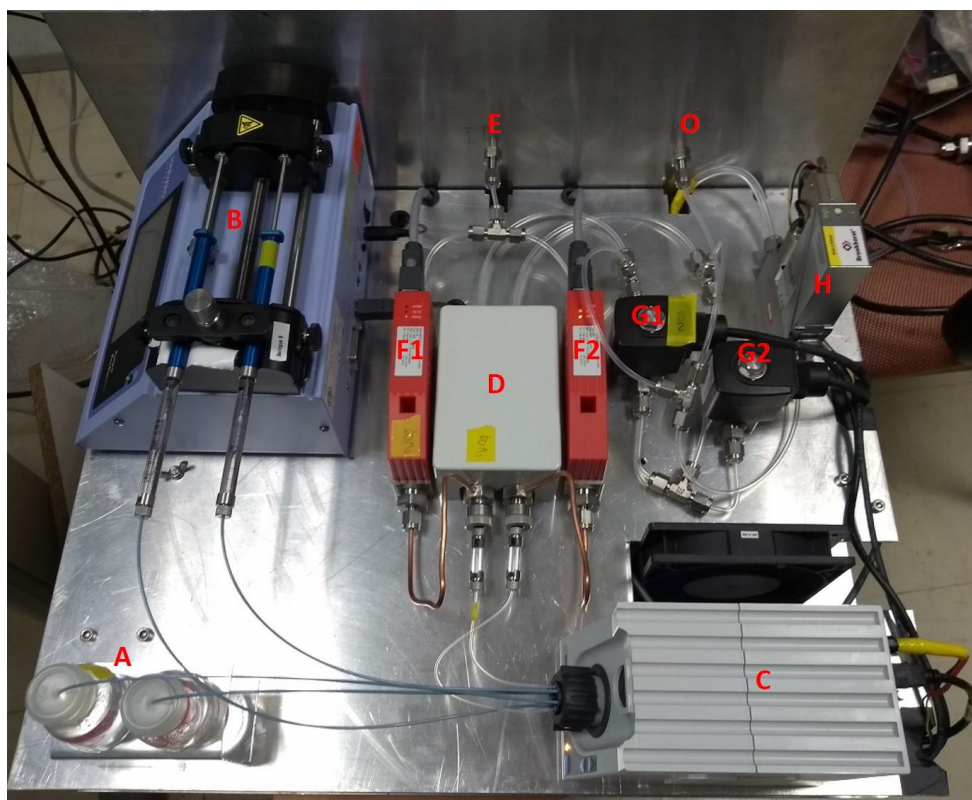
197

198   **_Figure 3_**: _Picture of the upper stage of the instrument with the main fluidic parts. Two water standards (A);_

199   _a dual syringe pump (B); a double three-way valve (C); two evaporation chambers (D); an input of dry air_

200   _(E); two high-precision mass flow controllers (F1 & F2); two electrovalves (G1 & G2); a pressure controller_

201   _(H); an outlet (O)._

202

203   -   **Software details**

204   The control software has been developed using open source Python libraries and homemade drivers,

205   including a user interface displaying the state of relevant components and the value of the different

206   sensors. The software (HumGen) can be downloaded on line (https://github.com/ojsd/humgen;

207   https://doi.org/10.5281/zenodo.4003465).

208 The LHLG can operate in eight different states, each state representing a specific setup for each element
209 (valves position, syringe pump infusion rate, dry air flow rate, pressure). Those eight states can be divided
210 into three categories: a simple mode, an expert mode and a humidity dependence calibration mode. The
211 simple mode is composed of six predefined states referring to the classical isotopic calibration in everyday
212 routine operation (Table 1): 1) measurement of the outside air water vapor isotopic composition; 2) drying
213 of the cavities; 3) "humidity boost", in order to reach faster the desired humidity level in the cavities; 4)
214 injection of the standard A in the corresponding evaporation chamber at a set humidity level; 5) injection
215 of the standard B in the corresponding evaporation chamber; 6) refill of the syringes. The expert mode is
216 useful to adjust each parameter manually: flow rates on the controllers F1 and F2, opening of the
217 electrovalves G1 and G2, mode (injection or refill) and infused rate for the syringe pump, pressure
218 regulation, state of the double three-way valve, activation of the vacuum pump at the exhaust, opening
219 of external electrovalves from the dry air tank and to the inlet (Figures 2 and 3). The humidity dependence
220 calibration mode produces a scale of increasing humidity steps in the evaporation chambers (e.g. from 100
221 ppmv to 1000 ppmv, through steps of 100 ppmv for 50 minutes for each standard). The details of the
222 sequence (standard type, humidity level and duration of each step) is defined in a text file by the operator
223 from the Raspberry interface, the Raspberry being itself connected to Ethernet for remote access.
224 The L2130-i analyser has an External Valve Sequencer, which is able to turn on/off up to six electrovalves
225 and create loop sequences with defined durations for each step of the sequence. This tool can be diverted
226 from its original purpose by using it as a 6-digit code: each of the humidity generator's state is associated
227 with a code. When the Picarro's Valve Sequencer matches one of the state's code, this state is triggered
228 on the humidity generator. This eases both the operator's activities and the data post-treatment, because
229 the current valve status - thus the calibration instrument state - is saved in the analyzer output data file,
230 in the "ValveMask" column. The Raspberry inside the LHLG reads the Valve Sequencer state code using
231 the Picarro's Remote Control Interface (a RS232 serial connection through one of the rear-face DB9
232 connector).
233

States (min)	Flow F1 (sccm)	Flow F2 (sccm)	Valve G1	Valve G2	Syringe Pump (µL/min)	Inlet Valve *	Dry air valve	Pressure controller (mbar)	Pressure Pump for exhaust	Double 3-way valve
Outside air (1100)	0	0	Closed	Closed	0	Open	Closed	Off	Off	To chamber
Drying (20)	400	400	Open	Open	0	Closed	Open	Off	Off	To chamber

Boost (0.7)	300	300	Open	Open	Infuse at 2.5	Closed	Open	905	On	To chamber
Standard A (50)	300	150	Open	Closed	Infuse at 0.25	Closed	Open	905	On	To chamber
Standard B (50)	150	300	Closed	Open	Infuse at 0.25	Closed	Open	905	On	To chamber
Reset (1)	Closed	Closed	Closed	Closed	Withdraw max speed	Open	Closed	Off	Off	From standard

234 ***Table 1***: *Typical routine sequence of measurements + calibration for two standards A and B at 1000 ppmv*

235 *for a measurement site located at sea level.*

236 *Note that the humidity dependence mode and the expert mode can also be included in the valve sequencer*

237 *but are not used in a daily calibration routine. *) The Inlet Valve is placed outside the vapor generator*

238 *instrument; when open it enables the measurement of outside air.*

239

240 A set of tools has been developed to quickly check daily calibration. In the field, analyzer and LHLG data

241 are archived daily and sent to the laboratory, i.e. at LSCE, Gif sur Yvette. They are checked semi-

242 automatically once a week to warn maintenance personnel in the event of a malfunction.

243

244 **3-   Performance of the instrument**

245 The LHLG is able to generate stable levels of humidity ranging from 70 ppmv to 2300 ppmv.

246 **3-1- No fractionation during water vaporization in the cavity**

247 We have checked that there was no fractionation of the water during its transfer from the bottles to the

248 the syringe pump, then from the syringe to the moist air generated in the vaporization chamber. The

249 isotopic composition of three different standards have been compared, generated by the present LHLG as

250 well as the commercial SDM, both at a humidity of 2,000 ppmv over 40-min time spans. The measured

251 $\delta^{18}O$ and δD excess values agreed to within 0.2‰ and 1‰, respectively, for the 3 standard waters. Note

252 that 2,000 ppmv is close to the upper value of the present LHLG (2,300 ppmv) while it is the very low one

253 of the SDM (see Fig. 6 of section 3-2).

254

255 **3-2- Stability of the water vapor delivery**
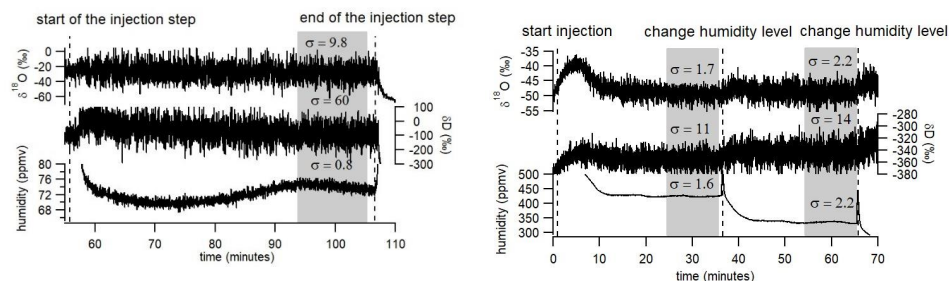
Figure 4: *Records of $\delta^{18}O$, δD and humidity over 3 humidity plateaus (72 ppmv on the left, 425 and 335 ppmv on the right) obtained with the LHLG (December 2018 at Concordia). The grey rectangles indicate the period (10 min) over which the average values are kept for calibrating the data generated by the* L2130-i *analyzer.*

Figure 4 displays the performance of the instrument at different low humidity levels (72, 425, and 335 ppmv). In the routine mode, we select the last 10 minutes before the following switch of the instrument to measure the average level of humidity and the isotopic ratios, $\delta^{18}O$ and δD. We also calculate the associated standard deviations and reject the values if the humidity standard deviation exceeds 30 ppm over these last 10 minutes. In Figure 4, one observes that the standard deviations for humidities generated are actually much lower, in the 2 ppm range. The corresponding standard deviations for the isotopic ratios ($\delta^{18}O$ and δD, see values indicated in Figure 4) increase with decreasing humidity, reflecting the molecular absorption signal decrease recorded by the Li2130-i laser analyzer. This has an obvious impact on the determination of the relationship between humidity and water vapor isotopic composition.

The performance of the present LHLG can be compared to the performance of the SDM. For such comparison, we used daily calibrations performed with a SDM, in a routine mode, during a 4.5 years field deployment in Svalbard (Leroy-Dos Santos et al., 2020). Over the full series, we kept only the 10-minute plateaus where standard deviation associated with humidity variations during calibration was below 150 ppmv. The best result at low humidity over the full period was a standard deviation σ of 31 ppmv over 10 minutes at 500 ppmv. Standard deviation largely increases when humidity decreases. This best SDM performance is significantly below the performance of the LHLG, which is a standard deviation 1-σ lower than 10 ppm on average and a 1-σ of 2 ppm for 30% of the generated humidity plateaus.

3-3- **Determination of the influence of humidity on water vapor isotopic composition**

280
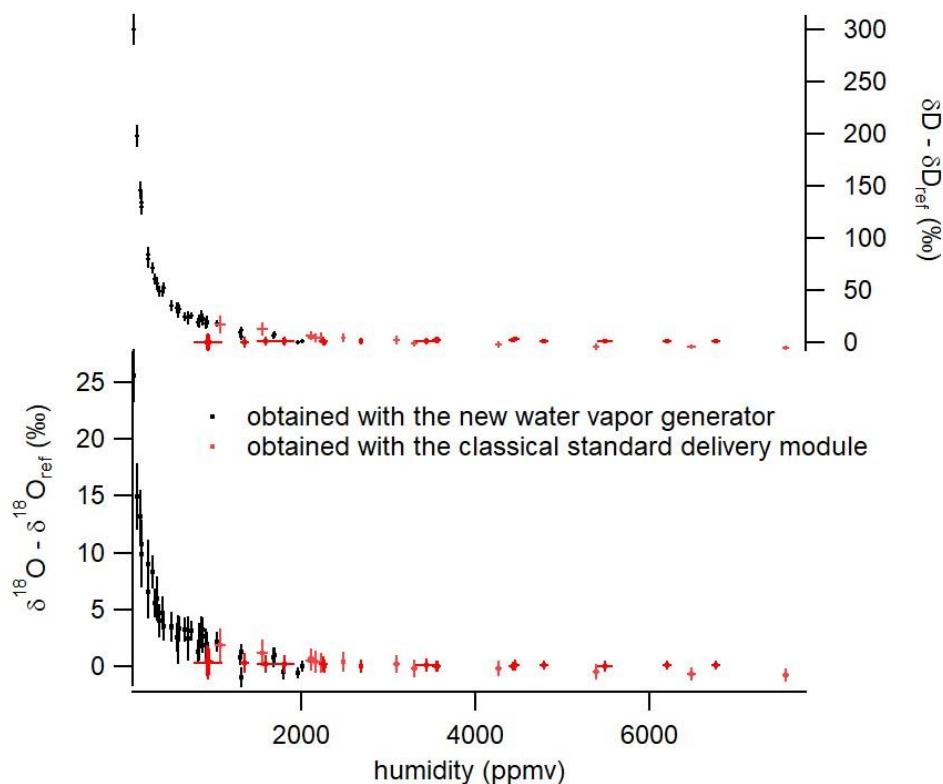
Figure 5: *Influence of humidity on the isotopic composition ($\delta^{18}O$ and δD) of the vapor obtained with a SDM*

281

(red) and with our new LHLG (black). The error bars are calculated as the standard deviation (1σ) over the

282

generated values by the L2130-i instrument at 1 second resolution (i.e. without any pre-averaging of the

283

raw dataseries). The $\delta^{18}O_{ref}$ and δD_{ref} are the true values of the injected water standards.

284

285

Contrary to the commercial SDM, which hardly produces stable and reproducible humidity levels below

286

500 ppmv, the LHLG was able to daily produce stable 10-minute humidity plateaus over the range from 70

287

ppmv to 2,000 ppmv with an associated standard deviation lower than 10 ppmv over more than one year

288

at the Concordia station (installation in December 2018). The stability of the LHLG allows a robust

289

quantification of the L2130-i analyzer drift thanks to a daily measurement of the same water isotopic

290

standard reference (Table 2). It also permits the characterization of the measurement nonlinearities

291

observed at low humidity (Figure 5). The more than one-year long Concordia dataset showed that the

292

humidity dependence of $\delta^{18}O$ and δD did not vary measurably. The uncertainty of the obtained calibration

293

curve can be attributed entirely to the L2130-i $\delta^{18}O$ and δD measurements. In other words, the uncertainty

294

bars in the horizontal (x-) axis for the black curve in Fig. 5, associated with the LHLG, are negligible.

295

296

Date	Humidity (ppmv)	$\delta^{18}O$ (‰)	δD (‰)
16 December 2019	380	-32.0	-207
17 December 2019	369	-31.9	-210
23 December 2019	371	-31.7	-212
24 December 2019	367	-31.9	-211
25 December 2019	378	-31.7	-211
26 December 2019	370	-31.7	-209
27 December 2019	386	-32.3	-208
28 December 2019	370	-31.5	-211
29 December 2019	364	-31.5	-209
30 December 2019	380	-31.7	-211
31 December 2019	372	-31.8	-211
1 January 2020	379	-31.8	-212
2 January 2020	371	-31.7	-211
3 January 2020	381	-31.6	-210
4 January 2020	378	-31.6	-210
5 January 2020	371	-31.6	-208

297

298 **_Table 2_**: _Example of daily measurements of humidity (1σ over 10 minutes = 9 ppmv), $\delta^{18}O$ (1σ over 10_

299 _minutes = 1.4 ‰), and δD (1σ over 10 minutes = 4.5 ‰) of a laboratory standard (NEEM) using the LHLG_

300 _at low humidity during the austral summer of 2019-2020._

301

302 **4-   Application**

303 The main application of this device is the interpretation of water isotopic profiles at dry sites, in particular

304 in polar regions. As shown in Figure 5, the influence of humidity on the measurement of the water vapor

305 isotopic composition with the L2130-i analyzer is large when humidity is below 2,000 ppm and increases

306 when humidity decreases. Even though the precise isotope ratio-humidity calibration curve is likely to be

307 different from one analyzer to another, all laser-based water isotope analyzers investigated to date have

308 shown a strongly non-linear response at low humidity levels (Guilpart et al., 2017; Leroy Dos-Santos, 2020;

309 Weng et al., 2020). At the Concordia station, even in summer, humidity is generally below 1000 ppm

310 (Figure 6) so that the interpretation of the diurnal variability of the water vapor isotopic composition is

311 strongly affected by the dependency of the measured $\delta^{18}O$ and δD signals on humidity. Figure 6 displays

312 such diurnal variabilities during austral summer 2018-2019 at Concordia and the consequently large

313 correction of the isotopic records (uncorrected in grey and corrected in black).

314
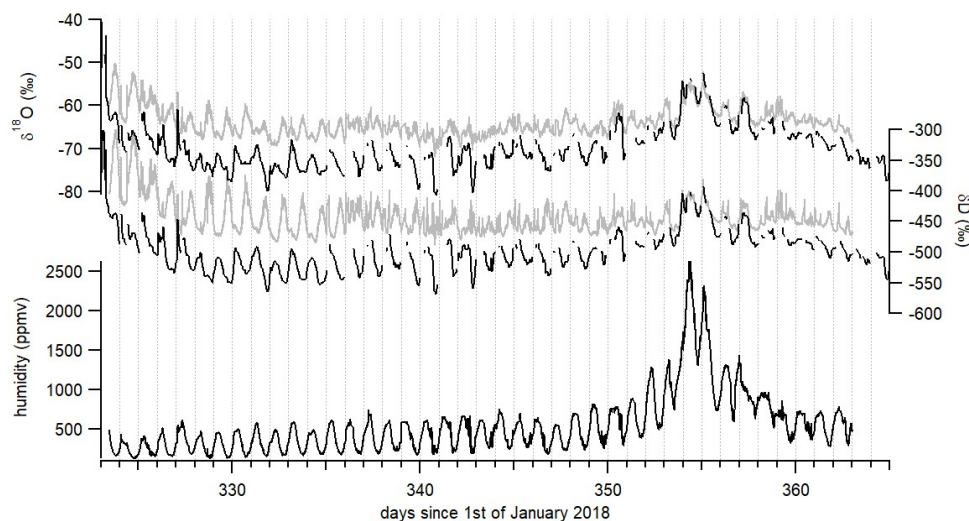
Figure 6: $\delta^{18}O$, δD and humidity records over December 2018 and beginning of January 2019. Raw isotopic

values are in grey. Corrected isotopic values at hourly resolution are in black after correction of the

influence of humidity on the water isotopic ratios and removal of measurements performed during

calibration or other maintenance operations.

319

The data clearly demonstrate the importance of the humidity correction which shifts the curves generally

to lower isotopic ratio values. However, the difference between uncorrected and corrected data is

particularly important in the observation of the diurnal variability, illustrated even better when zooming

in on a section of the data, as in Figure 7. When looking in detail at the diurnal variability in the raw $\delta^{18}O$

and δD isotope data, some periods stand out with two daily peaks identified, one in phase with the

humidity peak (marked in red in Figure 7) and one occurring during the period of minimum humidity

(marked in blue in Figure 7). The strong non-linearity of the calibration curve of Figure 5 suggests that

artificial peaks in $\delta^{18}O$ and δD could be due to changing humidity levels. Indeed, after correcting the data

for the humidity dependence of the analyzer (black curve in Figure 7), the isotopic peaks occurring during

humidity minima are diminished or disappear altogether, while the peaks occurring during humidity

maxima are amplified. More strikingly, the phase of the signal changes by practically 180° over some

periods. Whereas the raw isotope signal peaks during the night, the corrected record shows higher isotope

ratios during daytime. The diurnal variability recorded on both raw and corrected isotopic values during a

period with higher humidity level, hence when the isotope ratio-humidity correction is smaller (around

day 355 in figure 6), also shows that the $\delta^{18}O$ (δD) diurnal cycles are indeed in-phase with the humidity

cycle. This result confirms the correlation between humidity cycles and $\delta^{18}O$ and δD of the water vapor at

the daily scale at Concordia as reported by Casado et al. (2016). We thus conclude that the anticorrelation

337 observed between δ^{18}O (δD) and humidity in the raw data (highlighted in blue in Figure 7) during periods

338 of low humidity is an artefact due to the influence of the humidity level on the vapor isotopic

339 measurements by the L2130-i analyzer.
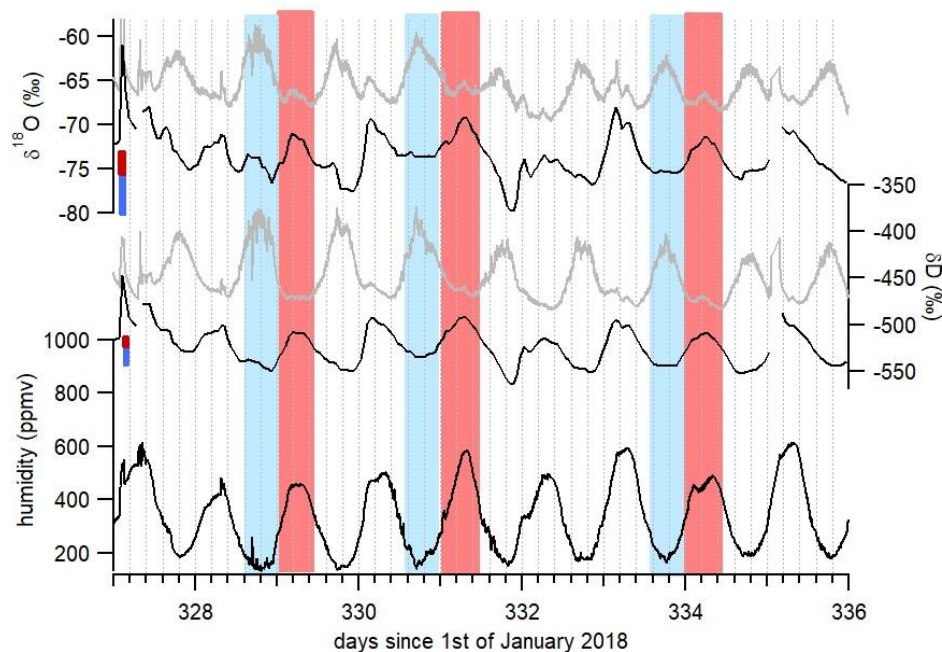
340

341 **_Figure 7_**: _Focus on diurnal variability of δ^{18}O, δD and humidity recorded at Concordia. Grey curves show the_

342 _raw measurements and black curves the corrected records. The red (blue) bars indicate the calculated_

343 _uncertainty due to the isotopes vs humidity dependence (Figure 5) on the corrected δ^{18}O and δD values_

344 _during periods with maximum (minimum) humidity. The red (blue) rectangles indicate half day with_

345 _maximum (minimum) humidity._

346

347 **5-   Conclusion**

348 We have developed an autonomous instrument for low humidity generation (70 to 2,300 ppmv) with

349 controlled water vapor isotopic composition specifically aiming at carrying out continuous measurements

350 of the water vapor isotopic composition using a laser-based spectrometer in regions characterized by very

351 low humidity, such as polar regions. An interface permits to conveniently connect the new LHLG to the

352 valve sequencer port of commercial Picarro instruments. After more than one year of routine operation

353 on two Antarctic sites (Dumont d'Urville and Concordia), this instrument has proven to be very reliable

354 and robust. It consistently generates stable humidity levels with a 1σ variability lower than 10 ppm over

355 more than 10 minutes. Besides, its performance is significantly better than that of the Picarro SDM at low

356 humidity.

357   We used this instrument for the calibration of our water isotopic data with a special focus on accurately

358   quantifying the influence of humidity on the measured isotopic composition of the water vapor. This effect

359   is huge at low humidity. We showed that this has an important impact on the interpretation of the diurnal

360   cycles of δ^{18}O and δD in the water vapor at the Concordia station at humidity below 1,500 ppmv. We were

361   able to confirm that, at this site, the diurnal δ^{18}O and δD variability is actually correlated with humidity

362   variability, which would not have been possible without the new LHLG instrument.

363   Finally, the development of such an instrument is an important step forward to a better understanding of

364   the transfer function between climate parameters and the isotopic composition of deep ice cores from

365   the remote East Antarctic plateau, especially in the context of the new program "Beyond EPICA". It should

366   be completed by ongoing development of laser spectrometers better adapted to low humidity levels, such

367   as those based on the technique of Optical Feedback Cavity Enhanced Absorption Spectroscopy (OFCEAS)

368   (Casado et al., 2016; Landsberg, 2014; Landsberg et al., 2014).

369

Author contributions

371   CLDS, MC, FP and EK designed and built the instrument. OJ realized the software interface development.

372   CLDS, MC and AL installed the instrument in Antarctica and tested it extensively. EK, SK and EF tested the

373   instrument in the laboratory. AL wrote the manuscript with the help of all co-authors.

374

Acknowledgments

376   The development presented in this manuscript is largely inspired from the initial PhD work of Janek

377   Landsberg which we gratefully acknowledge here. The research leading to these results has received

378   funding from the Antarctic Snow program of the Fondation Prince Albert II de Monaco, the ANR EAIIST and

379   CNRS-LEFE program ADELISE. The deployment of this instrument in the field was made possible through

380   the logistic support of the NIVO2 & ADELISE IPEV programs.

381

References

383   Aemisegger, F., Sturm, P., Graf, P., Sodemann, H., Pfahl, S., Knohl, A. and Wernli, H.: Measuring variations
384   δ^{18} O and δ^2 H in atmospheric water vapour using two commercial laser-based spectrometers: an
385   instrument characterisation study, Atmos. Meas. Tech., 5(7), 1491–1511, doi:10.5194/amt-5-1491-2012,
386   2012.

387   Bailey, H. L., Kaufman, D. S., Henderson, A. C. G. and Leng, M. J.: Synoptic scale controls on the δ^{18}O in
388   precipitation across Beringia, Geophys. Res. Lett., 42(11), 4608–4616,
389   doi:10.1002/2015GL063983.Received, 2015.

390   Bastrikov, V., Steen-Larsen, H. C., Masson-Delmotte, V., Gribanov, K., Cattani, O., Jouzel, J. and Zakharov,
391   V.: Continuous measurements of atmospheric water vapour isotopes in western Siberia (Kourovka),
392   Atmos. Meas. Tech., 7(6), 1763–1776, doi:10.5194/amt-7-1763-2014, 2014.

Bonne, J.-L., Masson-Delmotte, V., Cattani, O., Delmotte, M., Risi, C., Sodemann, H. and Steen-Larsen, H. C.: The isotopic composition of water vapour and precipitation in Ivittuut, southern Greenland, Atmos. Chem. Phys., 14(9), 4419–4439, doi:10.5194/acp-14-4419-2014, 2014.

Bréant, C., Leroy Dos Santos, C., Agosta, C., Casado, M., Fourré, E., Goursaud, S., Masson-Delmotte, V., Favier, V., Cattani, O., Prié, F., Golly, B., Orsi, A., Martinerie, P. and Landais, A.: Coastal water vapor isotopic composition driven by katabatic wind variability in summer at Dumont d'Urville, coastal East Antarctica, Earth Planet. Sci. Lett., 514, 37–47, doi:10.1016/j.epsl.2019.03.004, 2019.

Cappa, C. D., Hendricks, M. B., DePaolo, D. J. and Cohen, R. C.: Isotopic fractionation of water during evaporation, J. Geophys. Res., 108(D16), 4525, doi:10.1029/2003JD003597, 2003.

Casado, M., Landais, A., Masson-Delmotte, V., Genthon, C., Kerstel, E., Kassi, S., Arnaud, L., Picard, G., Prie, F., Cattani, O., Steen-Larsen, H.-C., Vignon, E. and Cermak, P.: Continuous measurements of isotopic composition of water vapour on the East Antarctic Plateau, Atmos. Chem. Phys. Discuss., 1–26, doi:10.5194/acp-2016-8, 2016.

Casado, M., Landais, A., Picard, G., Münch, T., Laepple, T., Stenni, B., Dreossi, G., Ekaykin, A., Arnaud, L., Genthon, C., Touzeau, A., Masson-Delmotte, V. and Jouzel, J.: Archival processes of the water stable isotope signal in East Antarctic ice cores, Cryosphere, 12(5), doi:10.5194/tc-12-1745-2018, 2018.

Dong, Feng, and Douglas Baer. 2010. "Development and Deployment of a Portable Water Isotope Analyzer for Accurate, Continuous and High-Frequency Oxygen and Hydrogen Isotope Measurements in Water Vapor and Liquid Water." In Geophysical Research Abstracts, 12:EGU2010-5571

Ellehoj, M. D., Steen-Larsen, H. C., Johnsen, S. J. and Madsen, M. B.: Ice-vapor equilibrium fractionation factor of hydrogen and oxygen isotopes: Experimental investigations and implications for stable water isotope studies, Rapid Commun. Mass Spectrom., 27(19), 2149–2158, doi:10.1002/rcm.6668, 2013.

Genthon, C., Piard, L., Vignon, E., Madeleine, J.-B., Casado, M. and Gallée, H.: Atmospheric moisture supersaturation in the near-surface atmosphere at Dome C, Antarctic Plateau, Atmos. Chem. Phys., 17(1), 691–704, doi:10.5194/acp-17-691-2017, 2017.

Gkinis, V., Popp, T. J., Johnsen, S. J. and Blunier, T.: A continuous stream flash evaporator for the calibration of an IR cavity ring-down spectrometer for the isotopic analysis of water, Isotopes Environ. Health Stud., 46(4), 463–475, doi:10.1080/10256016.2010.538052, 2010.

Guilpart, E., Vimeux, F., Evan, S., Brioude, J., Metzger, J., Barthe, C., Risi, C. and Cattani, O.: The isotopic composition of near-surface water vapor at the Maïdo observatory (Reunion Island, southwestern Indian Ocean) documents the controls of the humidity of the subtropical troposphere, J. Geophys. Res. Atmos., 122(18), 9628–9650, doi:10.1002/2017JD026791, 2017.

Iannone, R., Romanini, D., Kassi, S., Meijer, H. A. J. and Kerstel, E.: A Microdrop Generator for the Calibration of a Water Vapor Isotope Ratio Spectrometer, J. Atmos. Ocean. Technol., 26, doi:10.1175/2008JTECHA1218.1, 2009.

Jouzel, J., Masson-Delmotte, V., Cattani, O., Dreyfus, G., Falourd, S., Hoffmann, G., Minster, B., Nouet, J., Barnola, J. M., Chappellaz, J., Fischer, H., Gallet, J. C., Johnsen, S., Leuenberger, M., Loulergue, L., Luethi, D., Oerter, H., Parrenin, F., Raisbeck, G., Raynaud, D., Schilt, a, Schwander, J., Selmo, E., Souchez, R., Spahni, R., Stauffer, B., Steffensen, J. P., Stenni, B., Stocker, T. F., Tison, J. L., Werner, M. and Wolff, E. W.: Orbital and millennial Antarctic climate variability over the past 800,000 years., Science, 317(5839), 793–796, doi:10.1126/science.1141038, 2007.

434 Kopec, B., Lauder, A., Posmentier, E. and Feng, X.: The diel cycle of water vapor in west Greenland, J.
435 Geophys. Res. Atmos., 119(15), 9386–9399, 2014.

436 Landsberg, J.: Développement d'un spectromètre laser OF-CEAS pour les mesures des isotopes de la
437 vapeur d'eau aux concentrations de l'eau basses. [online] Available from:
438 http://www.theses.fr/2014GRENY052/document, 2014.

439 Landsberg, J., Romanini, D. and Kerstel, E.: Very high finesse optical-feedback cavity-enhanced absorption
440 spectrometer for low concentration water vapor isotope analyses., Opt. Lett., 39(7), 1795–1798,
441 doi:10.1364/OL.39.001795, 2014.

442 Lee, X., Sargent, S., Smith, R. and Tanner, B.: In Situ Measurement of the Water Vapor ^{18}O/^{16}O Isotope
443 Ratio for Atmospheric and Ecological Applications, J. Atmos. Ocean. Technol., 22(5), 555–565,
444 doi:10.1175/JTECH1719.1, 2005.

445 Leroy Dos Santos, C., Masson-Delmotte, V., Casado, M., Fourré, E., Steen-Larsen, H-C, Maturilli, M., Orsi,
446 A., Berchet, A., Cattani, O., Minster, B., Gherardi, J. and Landais, A., A 4.5 year-long record of Svalbard
447 water vapor isotopic composition documents winter air mass origin, J. Geophys. Research, in revision

448 Ritter, F., Steen-larsen, H. C., Werner, M., Masson-Delmotte, V., Orsi, A., Behrens, M., Birnbaum, G.,
449 Freitag, J., Risi, C. and Kipfstuhl, S.: Isotopic exchange on the diurnal scale between near-surface snow and
450 lower atmospheric water vapor at Kohnen station , East Antarctica, J. Geophys. Research (February), 1–
451 35, doi:10.5194/tc-2016-4, 2016.

452 Schmidt, M., Maseyk, K., Lett, C., Biron, P., Richard, P., Bariac, T. and Seibt, U.: Concentration effects on
453 laser-based δ^{18}O and δ^{2}H measurements and implications for the calibration of vapour measurements with
454 liquid standards, Rapid Commun. Mass Spectrom., 24(24), 3553–3561, doi:10.1002/rcm.4813, 2010.

455 Sodemann, H., Aemisegger, F., Pfahl, S., Bitter, M., Corsmeier, U., Feuerle, T., Graf, P., Hankers, R., Hsiao,
456 G., Schulz, H., Wieser, A. and Wernli, H.: The stable isotopic composition of water vapour above Corsica
457 during the HyMeX SOP1 campaign: Insight into vertical mixing processes from lower-tropospheric survey
458 flights, Atmos. Chem. Phys., 17(9), 6125–6151, doi:10.5194/acp-17-6125-2017, 2017.

459 Steen-Larsen, H. C., Masson-Delmotte, V., Hirabayashi, M., Winkler, R., Satow, K., Prié, F., Bayou, N., Brun,
460 E., Cuffey, K. M., Dahl-Jensen, D., Dumont, M., Guillevic, M., Kipfstuhl, S., Landais, A., Popp, T., Risi, C.,
461 Steffen, K., Stenni, B. and Sveinbjörnsdottír, A. E.: What controls the isotopic composition of Greenland
462 surface snow?, Clim. Past, 10(1), 377–392, doi:10.5194/cp-10-377-2014, 2014.

463 Sturm, P. and Knohl, A.: Water vapor δ ^{2}H and δ ^{18}O measurements using off-axis integrated cavity output
464 spectroscopy, Atmos. Meas. Tech. Discuss., 2(4), 2055–2085, doi:10.5194/amtd-2-2055-2009, 2009.

465 Tremoy, G., Vimeux, F., Cattani, O., Mayaki, S., Souley, I. and Favreau, G.: Measurements of water vapor
466 isotope ratios with wavelength-scanned cavity ring-down spectroscopy technology: new insights and
467 important caveats for deuterium excess measurements in tropical areas in comparison with isotope-ratio
468 mass spectrometry, Rapid Commun. Mass Spectrom., 25(23), 3469–3480, doi:10.1002/rcm.5252, 2011.

469 Wang, L., Caylor, K. and Dragoni, D.: On the calibration of continuous, high-precision δ^{18}O and δ^{2}H
470 measurements using an off-axis integrated cavity output spectrometer, Rapid Commun. Mass Spectrom.,
471 23, 530–536, doi:10.1002/rcm.3905, 2009.

472 Weng, Y., Touzeau, A. and Sodemann, H.: Impact of isotope composition on the humidity dependency
473 correction of water vapour isotope measurements with infra-red cavity ring-down spectrometers, Atmos.
474 Meas. Tech., 13, 3167–3190, https://doi.org/10.5194/amt-13-3167-2020, 2020.